Sensitivity enhancement in photonic crystal slab biosensors

Mohamed El Beheiry,[1] Victor Liu,[2] Shanhui Fan,[2] and Ofer Levi [1,3,*]

[1]*The Edward S. Rogers Sr. Department of Electrical and Computer Engineering, University of Toronto, 10 King's College Road, Toronto, Ontario M5S 3G4, Canada*
[2]*Department of Electrical Engineering, Stanford University, 420 Via Palou, Stanford, California 94305-4075, USA*
[3]*Institute of Biomaterials and Biomedical Engineering, University of Toronto, 164 College Street, Toronto, Ontario M5S 3G9, Canada*
**ofer.levi@utoronto.ca*

Abstract: Refractive index sensitivity of guided resonances in photonic crystal slabs is analyzed. We show that modal properties of guided resonances strongly affect spectral sensitivity and quality factors, resulting in substantial enhancement of refractive index sensitivity. A three-fold spectral sensitivity enhancement is demonstrated for suspended slab designs, in contrast to designs with a slab resting over a substrate. Spectral sensitivity values are additionally shown to be unaffected by quality factor reductions, which are common to fabricated photonic crystal nano-structures. Finally, we determine that proper selection of photonic crystal slab design parameters permits biosensing of a wide range of analytes, including proteins, antigens, and cells. These photonic crystals are compatible with large-area biosensor designs, permitting direct access to externally incident optical beams in a microfluidic device.

OCIS codes: (050.5298) Photonic crystals; (130.2790) Guided waves; (280.1415) Biological sensing and sensors; (170.4580) Optical diagnostics for medicine.

References and links

1. K. Shah, and R. Weissleder, "Molecular optical imaging: applications leading to the development of present day therapeutics," NeuroRx **2**(2), 215–225 (2005).
2. G. Iyer, F. Pinaud, J. Tsay, J. J. Li, L. A. Bentolila, X. Michalet, and S. Weiss, "Peptide coated quantum dots for biological applications," IEEE Trans. Nanobiosci. **5**(4), 231–238 (2006).
3. U. Resch-Genger, M. Grabolle, S. Cavaliere-Jaricot, R. Nitschke, and T. Nann, "Quantum dots versus organic dyes as fluorescent labels," Nat. Methods **5**(9), 763–775 (2008).
4. W. E. Moerner, "Single-molecule mountains yield nanoscale cell images," Nat. Methods **3**(10), 781–782 (2006).
5. X. Michalet, S. Weiss, and M. Jäger, "Single-molecule fluorescence studies of protein folding and conformational dynamics," Chem. Rev. **106**(5), 1785–1813 (2006).
6. F. Vollmer, and S. Arnold, "Whispering-gallery-mode biosensing: label-free detection down to single molecules," Nat. Methods **5**(7), 591–596 (2008).
7. X. Fan, I. M. White, S. I. Shopova, H. Zhu, J. D. Suter, and Y. Sun, "Sensitive optical biosensors for unlabeled targets: a review," Anal. Chim. Acta **620**(1-2), 8–26 (2008).
8. P. S. Cremer, "Label-free detection becomes crystal clear," Nat. Biotechnol. **22**(2), 172–173 (2004).
9. B. R. Schudel, C. J. Choi, B. T. Cunningham, and P. J. A. Kenis, "Microfluidic chip for combinatorial mixing and screening of assays," Lab Chip **9**(12), 1676–1680 (2009).
10. D. R. Shankaran, K. V. Gobi, and N. Miura, "Recent advancements in surface plasmon resonance immunosensors for detection of small molecules of biomedical, food and environmental interest," Sens. Actuators B Chem. **121**(1), 158–177 (2007).
11. J. Homola, "Present and future of surface plasmon resonance biosensors," Anal. Bioanal. Chem. **377**(3), 528–539 (2003).
12. V. Lirtsman, R. Ziblat, M. Golosovsky, D. Davidov, R. Pogreb, V. Sacks-Granek, and J. Rishpon, "Surface-plasmon resonance with infrared excitation: studies of phospholipid membrane growth," J. Appl. Phys. **98**(9), 093506 (2005).
13. R. Ziblat, V. Lirtsman, D. Davidov, and B. Aroeti, "Infrared surface plasmon resonance: a novel tool for real time sensing of variations in living cells," Biophys. J. **90**(7), 2592–2599 (2006).
14. I. M. White, and X. D. Fan, "On the performance quantification of resonant refractive index sensors," Opt. Express **16**(2), 1020–1028 (2008).

#131867 - $15.00 USD Received 19 Jul 2010; revised 7 Sep 2010; accepted 20 Sep 2010; published 12 Oct 2010

15. D. Erickson, S. Mandal, A. H. J. Yang, and B. Cordovez, "Nanobiosensors: optofluidic, electrical and mechanical approaches to biomolecular detection at the nanoscale," Microfluid Nanofluidics **4**(1-2), 33–52 (2008).
16. S. Zlatanovic, L. W. Mirkarimi, M. M. Sigalas, M. A. Bynum, E. Chow, K. M. Robotti, G. W. Burr, S. Esener, and A. Grot, "Photonic crystal microcavity sensor for ultracompact monitoring of reaction kinetics and protein concentration," Sens. Actuators B Chem. **141**(1), 13–19 (2009).
17. T. Xu, N. Zhu, M. Y. C. Xu, L. Wosinski, J. S. Aitchison, and H. E. Ruda, "A pillar-array based two-dimensional photonic crystal microcavity," Appl. Phys. Lett. **94**(24), 241110 (2009).
18. H. Ouyang, C. C. Striemer, and P. M. Fauchet, "Quantitative analysis of the sensitivity of porous silicon optical biosensors," Appl. Phys. Lett. **88**(16), 163108 (2006).
19. A. M. Armani, and K. J. Vahala, "Heavy water detection using ultra-high-Q microcavities," Opt. Lett. **31**(12), 1896–1898 (2006).
20. H. Altug, and J. Vucković, "Polarization control and sensing with two-dimensional coupled photonic crystal microcavity arrays," Opt. Lett. **30**(9), 982–984 (2005).
21. N. M. Hanumegowda, I. M. White, and X. D. Fan, "Aqueous mercuric ion detection with microsphere optical ring resonator sensors," Sens. Actuators B Chem. **120**(1), 207–212 (2006).
22. S. Tomljenovic-Hanic, A. Rahmani, M. J. Steel, and C. M. de Sterke, "Comparison of the sensitivity of air and dielectric modes in photonic crystal slab sensors," Opt. Express **17**(17), 14552–14557 (2009).
23. J. T. Robinson, L. Chen, and M. Lipson, "On-chip gas detection in silicon optical microcavities," Opt. Express **16**(6), 4296–4301 (2008).
24. M. R. Lee, and P. M. Fauchet, "Nanoscale microcavity sensor for single particle detection," Opt. Lett. **32**(22), 3284–3286 (2007).
25. F. Dell'Olio, and V. M. N. Passaro, "Optical sensing by optimized silicon slot waveguides," Opt. Express **15**(8), 4977–4993 (2007).
26. N. A. Mortensen, S. S. Xiao, and J. Pedersen, "Liquid-infiltrated photonic crystals: enhanced light-matter interactions for lab-on-a-chip applications," Microfluid. Nanofluid. **4**(1-2), 117–127 (2008).
27. S. Mandal, J. M. Goddard, and D. Erickson, "A multiplexed optofluidic biomolecular sensor for low mass detection," Lab Chip **9**(20), 2924–2932 (2009).
28. S. G. Johnson, S. H. Fan, P. R. Villeneuve, J. D. Joannopoulos, and L. A. Kolodziejski, "Guided modes in photonic crystal slabs," Phys. Rev. B **60**(8), 5751–5758 (1999).
29. S. Fan, and J. D. Joannopoulos, "Analysis of guided resonances in photonic crystal slabs," Phys. Rev. B **65**(23), 235112 (2002).
30. I. D. Block, N. Ganesh, M. Lu, and B. T. Cunningham, "Sensitivity model for predicting photonic crystal biosensor performance," IEEE Sens. J. **8**(3), 274–280 (2008).
31. O. Levi, M. M. Lee, J. Zhang, V. Lousse, S. R. J. Brueck, S. Fan, and J. S. Harris, "Sensitivity analysis of a photonic crystal structure for index-of-refraction sensing," Proc. SPIE **6447**, 1–9 (2007).
32. O. Levi, T. T. Lee, M. M. Lee, S. J. Smith, and J. S. Harris, "Integrated semiconductor optical sensors for cellular and neural imaging," Appl. Opt. **46**(10), 1881–1889 (2007).
33. M. Huang, A. A. Yanik, T.-Y. Chang, and H. Altug, "Sub-wavelength nanofluidics in photonic crystal sensors," Opt. Express **17**(26), 24224–24233 (2009).
34. L. Shi, P. Pottier, Y. A. Peter, and M. Skorobogatiy, "Guided-mode resonance photonic crystal slab sensors based on bead monolayer geometry," Opt. Express **16**(22), 17962–17971 (2008).
35. L. Shi, P. Pottier, M. Skorobogatiy, and Y.-A. Peter, "Tunable structures comprising two photonic crystal slabs--optical study in view of multi-analyte enhanced detection," Opt. Express **17**(13), 10623–10632 (2009).
36. S. H. Fan, "Sharp asymmetric line shapes in side-coupled waveguide-cavity systems," Appl. Phys. Lett. **80**(6), 908–910 (2002).
37. D. M. Whittaker, and I. S. Culshaw, "Scattering-matrix treatment of patterned multilayer photonic structures," Phys. Rev. B **60**(4), 2610–2618 (1999).
38. V. Liu, M. Povinelli, and S. Fan, "Resonance-enhanced optical forces between coupled photonic crystal slabs," Opt. Express **17**(24), 21897–21909 (2009).
39. A. F. Oskooi, D. Roundy, M. Ibanescu, P. Bermel, J. D. Joannopoulos, and S. G. Johnson, "MEEP: A flexible free-software package for electromagnetic simulations by the FDTD method," Comput. Phys. Commun. **181**(3), 687–702 (2010).
40. J. D. Joannopoulos, S. G. Johnson, J. N. Winn, and R. D. Meade, *Photonic Crystals: Molding the Flow of Light*, Second ed. (Princeton University Press, Princeton, NJ, 2008).
41. O. Kilic, S. Kim, W. Suh, Y. A. Peter, A. S. Sudbø, M. F. Yanik, S. H. Fan, and O. Solgaard, "Photonic crystal slabs demonstrating strong broadband suppression of transmission in the presence of disorders," Opt. Lett. **29**(23), 2782–2784 (2004).
42. Y. Nazirizadeh, U. Lemmer, and M. Gerken, "Experimental quality factor determination of guided-mode resonances in photonic crystal slabs," Appl. Phys. Lett. **93**(26), 261110 (2008).
43. I. D. Block, M. Pineda, C. J. Choi, and B. T. Cunningham, "High Sensitivity Plastic-Substrate Photonic Crystal Biosensor," IEEE Sens. J. **8**(9), 1546–1547 (2008).
44. J. Homola, I. Koudela, and S. S. Yee, "Surface plasmon resonance sensors based on diffraction gratings and prism couplers: sensitivity comparison," Sens. Actuators B Chem. **54**(1-2), 16–24 (1999).
45. J. Hu, X. Sun, A. Agarwal, and L. C. Kimerling, "Design guidelines for optical resonator biochemical sensors," J. Opt. Soc. Am. B **26**(5), 1032–1041 (2009).
46. J. Homola, S. S. Yee, and G. Gauglitz, "Surface plasmon resonance sensors: review," Sens. Actuators B Chem. **54**(1-2), 3–15 (1999).

#131867 - $15.00 USD Received 19 Jul 2010; revised 7 Sep 2010; accepted 20 Sep 2010; published 12 Oct 2010

47. Y. Fang, A. M. Ferrie, N. H. Fontaine, J. Mauro, and J. Balakrishnan, "Resonant waveguide grating biosensor for living cell sensing," Biophys. J. **91**(5), 1925–1940 (2006).
48. L. L. Chan, S. L. Gosangari, K. L. Watkin, and B. T. Cunningham, "A label-free photonic crystal biosensor imaging method for detection of cancer cell cytotoxicity and proliferation," Apoptosis **12**(6), 1061–1068 (2007).
49. M. F. Pineda, L. L. Y. Chan, T. Kuhlenschmidt, C. J. Choi, M. Kuhlenschmidt, and B. T. Cunningham, "Rapid Specific and Label-Free Detection of Porcine Rotavirus Using Photonic Crystal Biosensors," IEEE Sens. J. **9**(4), 470–477 (2009).
50. W. Zhang, N. Ganesh, P. C. Mathias, and B. T. Cunningham, "Enhanced fluorescence on a photonic crystal surface incorporating nanorod structures," Small **4**(12), 2199–2203 (2008).
51. E. Thrush, O. Levi, L. J. Cook, J. Deich, A. Kurtz, S. J. Smith, W. E. Moerner, and J. S. Harris, Jr., "Monolithically integrated semiconductor fluorescence sensor for microfluidic applications," Sens. Actuators B Chem. **105**(2), 393–399 (2005).
52. O. Andersson, A. Larsson, T. Ekblad, and B. Liedberg, "Gradient hydrogel matrix for microarray and biosensor applications: an imaging SPR study," Biomacromolecules **10**(1), 142–148 (2009).

1. Introduction

The ability to detect biologically active molecules is of crucial importance for fundamental studies in biochemistry, applications in drug development, and point-of-care diagnostics. Medical diagnostics often rely on slow, labor-intensive, and expensive optical laboratory techniques. The miniaturization of biological analysis systems based on micro-channels and micro-arrays promises to facilitate portable detection of common diseases, and to greatly enhance diagnosis. In many cases, detection of biomolecules is assisted by labels or tags (e.g. radioactive, fluorescent) [1–3]. Such methods can allow very sensitive detection in bio-assays, which are capable of detecting single molecules [4,5]. Labels, however, can structurally and functionally interfere with analyte molecules, and may not be specific. Label-free approaches allow rapid real-time detection in small volumes with minimal sample preparation, which is compatible with small clinics and field evaluation [6].

Label-free biosensing can be based on the localization of capture molecules (e.g. peptides and antibodies) on a treated surface or on a small bead [7–9]. In general, label-free biosensing with optics relies on detecting changes in a local parameter such as absorption, refractive index (RI), or scattering. Common devices for localized RI sensing are commercially available surface plasmon resonance (SPR) sensors, which sense RI changes near a metal surface by measuring reflectivity changes due to modified coupling of incident light to surface plasmons [10,11]. Due to the short decay length of the evanescent electromagnetic fields, the probing depth for SPR sensors is generally limited to ~100nm above the metal surface in aqueous media. This technique has been extended to longer IR wavelengths where lower losses in thin gold layers result in sharper resonance dips [12] and longer penetration depths (as much as a few microns) permitting interrogation of organelles inside live cells [13]. However, SPR and metal-based detection methods suffer from intrinsic losses, and often involve complex means for coupling incident beams, limiting the flexibility and portability of such devices. In addition, the inherently low quality factors (Q) of SPR sensors increase ambiguity when determining the spectral resonance location in the presence of spectral noise [14].

Nanoscale biosensors can offer advantages over traditional sensing techniques that offset the complexity and cost involved in their construction [15]. In many nanoscale and microscale resonance-based systems for localized RI sensing, the captured analyte molecules are located within the evanescent electromagnetic field regions near a dielectric surface. Cavities of various architectures have been used to detect analyte molecules [16–26]. Furthermore, staggering clusters of capture molecules next to each other allows for detection of multiple analyte molecules [27]. In many instances, however, high-Q cavity and waveguide-based sensing approaches require delicate alignment schemes, have low coupling efficiencies from free space optical beams, and may suffer from extreme temperature sensitivity [14].

An important class of nanoscale biosensors are photonic crystal slab (PCS) devices. A PCS is a one- or two-dimensional periodically patterned dielectric slab. The light can be confined to in-plane guided modes by the higher RI dielectric material (with no coupling to externally incident optical beams) [28] or can be confined to guided resonance modes in the slab, where coupling to externally incident optical beams is allowed [29]. Using guided

#131867 - $15.00 USD Received 19 Jul 2010; revised 7 Sep 2010; accepted 20 Sep 2010; published 12 Oct 2010

resonance modes for sensing is very appealing when easy coupling to externally incident beams in a microfluidic system for biosensing is desired.

In the past decade, several groups have studied the applications of photonic crystal (PC) structures for RI sensing. Studies of one-dimensional periodically patterned dielectric slab (grating) devices for biosensing applications show good sensitivity values, simplified light coupling schemes, and compatibility with plastic substrates [9,30]. However, one-dimensional grating structures are very sensitive to incoming light polarization, which reduces efficiency and requires careful polarization stabilization of the light source. Accordingly, many recent research efforts have focused on the study of two-dimensional planar PC structures, where light is coupled to in-plane guided modes from the narrow facet of a slab, as the review by Mortensen *et al.* describes [26]. Coupling light into such PC structures is challenging as a matching waveguide section may be needed to couple between the free space incident beam and the small mode size inside the PC structure.

We have experimentally demonstrated the use of guided resonance modes in PCS RI sensors for biosensing applications where light coupling to the PCS is greatly simplified [31,32]. It was recently shown that free-standing PCS films interacting with small fluid volumes can enhance analyte transport to potentially improve RI sensing [33]. Furthermore, theoretical studies of guided resonance modes for biosensing have evaluated a PCS embedded with spherical voids to capture analytes as well as using a pair of PCS structures as tunable dielectric mirrors to enhance sensitivity [34,35].

A specific discussion on the modal sensing attributes of PCS biosensors has not been previously reported, to our knowledge. As will be elaborated, the nature of the PCS guided mode has significant implications regarding spectral sensitivity, limit of detection, substrate presence, and the range of detectable analytes.

In this work, we emphasize the theoretical properties of RI sensing in PCS devices to complement recent realizations of photonic crystal-based sensor devices. We evaluate previously unreported properties for guided resonance modes in these devices and determine that the type of guided resonance mode supported by the PCS (TE- or TM-like) can result in significantly different sensing characteristics. This difference is especially significant in symmetric PCS structures, where the slab is suspended in water.

This paper is organized as follows. In Section 2, we discuss the computational techniques by which the analysis in this paper is based. Section 3 provides the figures of merit and metrics that are used to evaluate the different sensor configurations. Section 4 describes TE- and TM-like guided resonance modes in PCS devices. Section 5 compares several PCS designs, and provides estimates for sensitivity and Q values in practically realizable configurations such as symmetric (suspended slab) and asymmetric (slab on a silicon dioxide substrate) architectures. Finally, Section 6 discusses biosensing implications.

2. Computational methods

Our analysis focuses on PCS structures, the periodically patterned dielectric slabs described in Fig. 1. A PCS may be entirely described by a unit cell with a lattice constant, a, an associated hole radius, r, and slab thickness, t, seen in Fig. 1 (a). We analyze PCS structures made of a high-index material, silicon nitride (SiN_x, n = 2.00), immersed in a low-index fluid, such as water (n = 1.33). In the symmetric case shown in Fig. 1 (b), the SiN_x PCS is surrounded by water from above and below. In the asymmetric case shown in Fig. 1 (c), it is resting on a silicon dioxide (SiO_2, n = 1.46) substrate. Excitation is a normally incident plane wave (along the z-direction) with an electric field linearly polarized along the y-direction. The effects described here are general and apply to incident wave polarization along the x-direction as well. The transmission spectra for a typical PCS design include sharp Fano resonances, as shown in Fig. 1 (d), superimposed on a smoothly varying background similar to the transmission response obtained from a Fabry-Pérot etalon [36]. The properties of these guided resonances will be discussed below in Section 4.

#131867 - $15.00 USD Received 19 Jul 2010; revised 7 Sep 2010; accepted 20 Sep 2010; published 12 Oct 2010

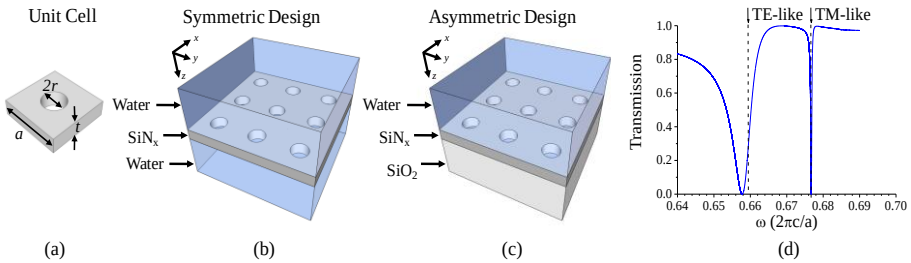

Fig. 1. (a) A unit cell for a square grid of holes PCS. Illustrations of (b) symmetric and (c) asymmetric PCS designs. (d) A typical transmission spectrum for a PCS with guided resonance frequencies indicated by dashed lines.

Throughout this work, we compare two independent computational techniques to evaluate the resonance behavior of our PCS structures. The first technique is a scattering matrix method (SMM) used to compute transmission through the slab, *Q* values, and spectral sensitivity ($\Delta\lambda/\Delta n$) by tracking shifts in guided resonances. This particular SMM technique is based on the implementations proposed by Whittaker and Culshaw [37], further details of which are provided in [38].

The second computational technique used is Meep, a freely available finite-difference time-domain implementation [39]. Meep allows three-dimensional PCS structures to be simulated with the use of periodic boundary conditions (PBCs) and perfectly matched layers (PMLs) applied to the unit cell. PBCs are applied to the *xz* and *yz* planes to emulate infinite planar periodicity, while PMLs terminate the top and bottom of the unit cell to absorb outgoing fields. To solve modes of the PCS, the excitation consists of a broadband planar Gaussian source located above the PCS. Modal field distributions are calculated by exciting the PCS using a planar continuous-wave source also located above the PCS. Meep was used to calculate the instantaneous field energies and distributions, which are used to evaluate the sensing metrics presented in Section 3.

3. Measures of sensitivity

The sensing mechanism in our PCS sensors is the detected shifts in the spectral location of guided resonances. This shift comes from changes in the RI of the medium surrounding the PCS. As a method of biosensing, the PCS surface may be coated with a thin layer of biorecognition molecules that bind specifically to an analyte (for example, antibodies with affinity to a specific protein, or streptavidin with an affinity to biotin). When excited at a guided resonance frequency, the PCS will have significant electric field energy engulfing the biorecognition layer. In an aqueous environment, such as in a flow channel, analytes binding to the biorecognition layer will cause a change in the local RI of that region [15]. This RI change will, in turn, induce a detectable spectral shift of the PCS guided resonances.

The relationship between small changes in RI of the surrounding medium and the shift in guided resonance frequency is linear to a first-order approximation. An important metric in quantifying this shift is the filling fraction or optical overlap integral, *f*, which describes the ratio of electric field energy existing outside of a dielectric structure with the total at a given mode [26]:

$$f = \frac{\int_{V_{liquid}} \varepsilon \left|\vec{E}\right|^2 dr^3_{liquid}}{\int_{V_{liquid+dielectric}} \varepsilon \left|\vec{E}\right|^2 dr^3_{liquid+dielectric}}. \quad (1)$$

The volume integral in the numerator of Eq. (1) gets contributions only from the liquid regions, where due to analyte binding there is a small perturbation, $\Delta\varepsilon$, to the otherwise linear

#131867 - $15.00 USD Received 19 Jul 2010; revised 7 Sep 2010; accepted 20 Sep 2010; published 12 Oct 2010

and unperturbed dielectric function ε [40]. Assuming that $\Delta n/n$ is the same for all perturbed liquid regions and following the perturbation theory arguments presented by Mortensen *et al*. [26], we introduce a bulk spectral sensitivity variable, S (in nm/RIU), and relate it to the predicted spectral shift, $\Delta\lambda$, in resonance wavelength, λ_0, due to a change in RI, Δn, of the liquid medium by:

$$S = \frac{\Delta\lambda}{\Delta n_{liquid}} = f\,\frac{\lambda_0}{n_{eff}} \quad \left[\frac{\text{nm}}{\text{RIU}}\right], \tag{2}$$

where n_{eff} is the effective RI of the dielectric sensing structure. Consequently, based on Eqs. (1) and (2), it is recognized that a large f value implies a considerable electric field energy in locations outside the dielectric structure (in our case, the SiN_x PCS) available for sensing changes in RI. We note that this calculation assumes that a small perturbation in RI does not change the mode significantly [40]. This analytical approach is evaluated with Meep and compares very well to transmission resonance sensitivity evaluation using the SMM, as will be presented later. In addition to S, we define the sensor spectral resolution, R, and the detection limit, DL, which describes the smallest spectral shift and the smallest RI change that may be measured with an RI sensor, respectively [14]:

$$DL = \frac{R}{S} = k\frac{\Delta\omega}{S} = k\frac{\omega_0}{QS} \quad [\text{RIU}], \tag{3}$$

where $\Delta\omega$ and ω are the full-width half-maximum spectral bandwidth and frequency of the guided resonance, respectively. It is noted that the DL is inversely related to Q (defined traditionally as $Q = \omega_0 / \Delta\omega$). The proportionality constant, k, relates the spectral resolution R to the resonance bandwidth by $R = k\cdot\Delta\omega$. We note that k is dependent on the spectral lineshape, and the signal-to-noise ratio (SNR) in the measurement system. In conventional single mode cavities, the reflectivity lineshape is typically a symmetric Lorentzian lineshape, however, in a PCS, a much sharper asymmetric lineshape can be realized [36]. The SNR for a measurement can be improved by increasing the measurement duration and subsequently, k values will change by modifying the SNR in the optical measurement. The DL is an important measure in practice since the ability to measure spectral shifts depends on both S and the shape of the resonance feature.

4. Guided resonance modes

The PCS biosensors in this work sense by observing changes in guided resonance frequencies. In a uniform dielectric slab, guided modes are confined to the slab and are uncoupled to the continuum of radiation modes that exist outside of it. However, the introduction of a two-dimensional periodic lattice of holes in the slab, constituting a PCS, provides a phase-matching mechanism which allows guided and radiation modes to couple, forming guided resonances [29]. In a reduced-zone band diagram, a guided resonance is described as a guided mode that folds at the Brillouin zone edge and exists above the light line, hence, coupling to radiation modes. In a transmission spectrum, coupling to a guided resonance results in sharp Fano lineshapes which have finite lifetimes described by widely varying Q values. The PCS architecture (symmetric or asymmetric, as shown in Fig. 1) is an important parameter in PCS biosensor optimization. The underlying SiO_2 substrate can be etched away to create a symmetric device with water above and below the PCS. Creating such a suspended slab membrane can complicate sensor fabrication [41] and introduce stress-related issues to the PCS, which may influence sensing properties. A suspended slab can also present major benefits such as shorter analyte detection times and increased sensitivity due to an enlarged biosensing volume. Therefore, we consider both device architectures as part of this work. In this section, we will focus our analysis on the nature of guided resonance modes in symmetric PCS designs. In the subsequent section, we will show that our analysis and main conclusions hold for asymmetric PCS designs as well.

A normally-incident plane wave may excite TE- or TM-like modes [28] as shown in Figs. 2 and 3. Following the convention in [28], TE- and TM-like modes have even or odd

#131867 - $15.00 USD Received 19 Jul 2010; revised 7 Sep 2010; accepted 20 Sep 2010; published 12 Oct 2010

symmetry, respectively, in their electric field with respect to the mirror plane perpendicular to the vertical (z) axis. Since a plane wave incident from one side of a slab does not respect such mirror plane symmetry, it can couple to both TE- or TM-like modes. This property is unique to guided resonances as both types of modes can be excited by a normally incident external beam.

A PCS excited at a TE-like guided resonance frequency will have its dominant electric field component coincident with that of the excitation (i.e. along the y-direction for an incident beam polarized in the y-direction), seen in Fig. 2 (b). The periodic hole pattern (which introduces a periodic RI modulation) seen by the in-plane electric field will result in considerable scattering and a short resonating lifetime (low Q). Hence, much of the electric field energy, $\varepsilon|E|^2$, shown in Fig. 2 (a), is restricted to the dielectric and hole regions of the slab in TE-like resonance conditions. Figure 2 (c) shows transmission spectra for symmetric PCS designs of different hole radii excited at TE-like guided resonance frequencies. Increasing the hole radius-to-period ratio (r/a) increases light scattering in the PCS, reducing associated Q values. In addition, the increased (r/a) ratio introduces a larger amount of electric field energy into the hole region, therefore increasing the f values.

In contrast, the electric field energy in TM-like guided-resonances is greatly extended into the media above and below the slab, as shown in Fig. 3 (a). A considerable portion of the electric field energy is localized normally to the SiN_x slab, producing a strong vertical electric field penetration. The plots in Fig. 3 (b) support this analysis, where the dominant electric field component is seen to be in the direction normal to the PCS surface (along the z-direction). The confinement of the mode to the dielectric slab region and the contribution of in-plane scattering effects are both reduced, giving rise to long resonating lifetimes and high Q values. The transmission spectra, shown in Fig. 3 (c) for a TM-like guided resonance in a symmetric PCS, show a trend of increasing Q values with decreasing (r/a) ratios, similar to the TE-like case. The narrower transmission linewidths of TM-like guided resonances, in comparison to TE-like conditions, indicates that a lower spectral shift would be required to detect bound analytes to the PCS surface. Moreover, the electric field energy is primarily located outside the slab region, suggesting smaller changes in f values with increasing (r/a) ratios should be anticipated, as compared to TE-like guided resonances. Importantly, the vertical confinement of the electric field suggests that PCS biosensors operating at a TM-like guided resonance will be significantly less sensitive to hole roughness and fabrication-related imperfections, effects which are often unavoidable in nanofabrication. This may overcome many of the current experimental challenges in realizing high Q devices in large area PCS biosensors.

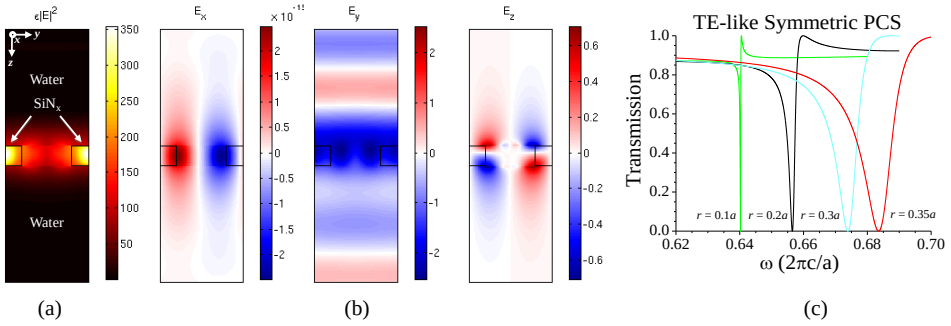

Fig. 2. TE-like guided resonance mode profile in a symmetric PCS: (a) the electric field energy density, $\varepsilon|E|^2$, and (b) field profile components (E_x, E_y, E_z). The electric field and electric field energy density profiles were calculated using the SMM method for a hole radius to period ratio (r/a) = 0.3. (c) TE-like mode transmission spectrum for hole radius r = 0.1a, 0.2a, 0.3a, and 0.35a. Units for the electric field and electric field energy are arbitrary and consistent between plots.

#131867 - $15.00 USD Received 19 Jul 2010; revised 7 Sep 2010; accepted 20 Sep 2010; published 12 Oct 2010

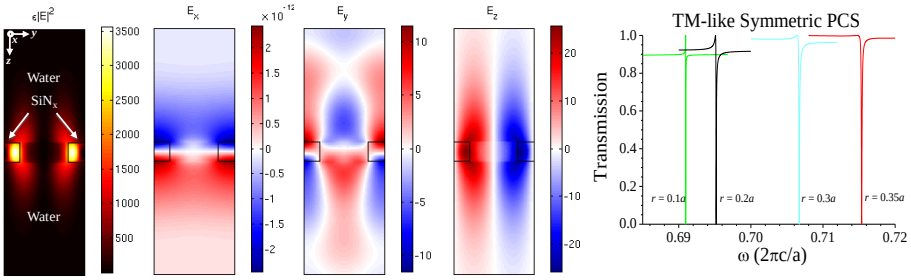

Fig. 3. TM-like guided resonance mode profile in a symmetric PCS: (a) the electric field energy density, $\varepsilon|E|^2$, and (b) field profile components (E_x, E_y, E_z). The electric field and electric field energy density profiles were calculated using the SMM method for a hole radius to period ratio (r/a) = 0.3. (c) TM-like mode transmission spectrum for hole radius r = 0.1a, 0.2a, 0.3a, and 0.35a.

The consequence of high Q values and strong field penetration (large f) on sensitivity will be discussed in Section 6. In the cases we have evaluated, the fundamental TM-like guided-resonance mode is observed in frequencies higher than those of the fundamental TE-like guided resonance.

A summary of the mode properties for the TE- and TM-like guided resonance modes from Fig. 2 (c) and 3 (c) is shown in Table 1. For illustrative purposes, we have defined a = 1000 nm to set normalized frequencies, ω_0, to wavelengths, λ_0, roughly in the communication band. The S values are calculated using the SMM technique (by tracking resonances in transmission) and using Meep (using Eq. (2)). Both methods are in good agreement.

In a TE-like case, when the hole diameter is increased, n_{eff} of the PCS is reduced, enabling more electric field energy to interact with the immersing fluid, hence, increasing f and S. This effect is moderate. The large increase in S observed in Table 1 for the TM-like case compared to the TE-like case, correlates well with the significant electric field energy penetration in water, seen in Fig. 3 (a), and the high f values. The spectral sensitivities observed in the TM-like case are largely invariant to the hole diameter. As discussed above, the electric field energy is primarily located outside the slab region, suggesting smaller changes in f and S values with increasing (r/a) ratios as compared to the TE-like case.

The trend of decreasing Q values with increasing (r/a) ratios is easily observed for both TE- and TM-like guided resonance modes in Figs. 2 (c), 3 (c) and the values listed in Table 1. When the hole diameter is increased, scattering within the slab is effectively increased, resonance lifetime is decreased and a lower Q value is the end result.

Decreasing the PCS slab thickness, shown in the bottom row of Table 1, results in slightly higher penetration of the electric field energy into the water, increasing f and S. The supported guided mode equally extends to both sides of the slab and has a slightly higher S than in the thicker slab cases.

Table 1. Sensitivity values for symmetric PCS designs of different radius holes. Indicated are the guided resonance wavelengths, bulk sensitivity values calculated from SMM and Meep, filling fractions, and quality factors for TE- and TM-like conditions.

Hole Radius [nm]	TE-like					TM-like				
	λ_0 [nm]	S_{SMM} [nm/RIU]	S_{Meep} [nm/RIU]	f	Q	λ_0 [nm]	S_{SMM} [nm/RIU]	S_{Meep} [nm/RIU]	f	Q
100	1561	381	313	0.336	3513	1447	764	728	0.736	110601
200	1520	456	411	0.435	313	1438	777	709	0.715	16240
300	1479	549	564	0.580	95	1415	805	743	0.753	10430
350	1457	599	643	0.654	68	1398	829	777	0.788	11984
300 (t=180 nm)	1438	644	656	0.675	125	1376	902	875	0.877	71761

Importantly, Table 1 shows that modal properties of guided resonances strongly affect S and Q, and result in enhancement of RI sensitivity for the TM-like guided resonance modes.

#131867 - $15.00 USD Received 19 Jul 2010; revised 7 Sep 2010; accepted 20 Sep 2010; published 12 Oct 2010

5. Asymmetric structures

Many of the recent experimental studies concerning photonic crystal based sensing structures incorporate an asymmetric topology, where the photonic crystal layer rests on a dielectric substrate, such as SiO_2 [20,31,42,43] The main motivation for asymmetric PCS implementations is the significantly reduced fabrication challenge, in comparison to the symmetric, suspended PCS designs discussed in Section 4. In light of this, we contrast the sensing attributes of the two design types.

Figures 4 and 5 illustrate the electric field energy density and the electric field mode profiles for the fundamental (lowest-order) TE- and TM-like guided resonances in an asymmetric PCS design, respectively. Mode profiles correspond closely to those of the symmetric design. The asymmetric design does, however, introduce a RI contrast with the substrate that is smaller than that of the water superstrate. The result is that most of the evanescent field energy exists in the substrate, greatly affecting sensing characteristics.

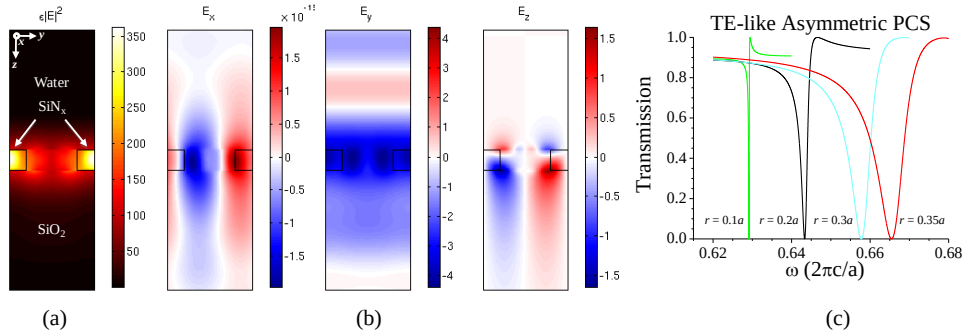

Fig. 4. TE-like guided resonance mode profile in an asymmetric PCS: (a) the electric field energy density, $\varepsilon|E|^2$, and (b) field profile components (E_x, E_y, E_z). The electric field and electric field energy density profiles were calculated using the SMM method for a hole radius to period ratio (r/a) = 0.3. (c) TE-like mode transmission spectrum for hole radius r = 0.1a, 0.2a, 0.3a, and 0.35a.

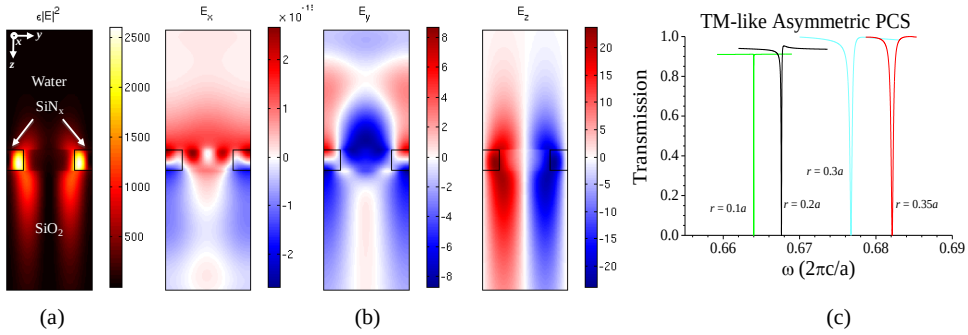

Fig. 5. TM-like guided resonance mode profile in an asymmetric PCS: (a) the electric field energy density, $\varepsilon|E|^2$, and (b) field profile components (E_x, E_y, E_z). The electric field and electric field energy density profiles were calculated using the SMM method for a hole radius to period ratio (r/a) = 0.3. (c) TM-like mode transmission spectrum for hole radius r = 0.1a, 0.2a, 0.3a, and 0.35a.

A summary of the mode properties for the TE- and TM-like guided resonance modes from Figs. 4 (c) and 5 (c) is shown in Table 2. The reduced electric field energy penetration into water results in reductions in f and S, compared to the corresponding guided resonances in the symmetric designs. The TE-like S is roughly halved as compared to the symmetric design values in Table 1. Effectively, we have removed half the volume where fields are able to interrogate the fluid for analyte presence, so we expect to see a similar reduction in S. As observed in Fig. 5 (a), due to the small RI contrast between the PCS and the substrate, most of

#131867 - $15.00 USD Received 19 Jul 2010; revised 7 Sep 2010; accepted 20 Sep 2010; published 12 Oct 2010

the electric field energy outside the slab is localized in the substrate. This leads to much lower *f* and S values.

Importantly, for the same TM-like guided resonance, the spectral sensitivity is three times higher for the symmetric design than the asymmetric design. This implies that in addition to a larger effective sensing area to accumulate analytes, symmetric designs possess an intrinsically smaller *DL* due to their modal properties.

Table 2. Sensitivity values for asymmetric PCS designs of different radius holes. Indicated are the guided resonance wavelengths, bulk sensitivity values calculated from SMM and Meep, filling fractions, and quality factors for TE- and TM-like conditions.

Hole Radius [nm]	TE-like					TM-like				
	λ_0 [nm]	S_{SMM} [nm/RIU]	S_{Meep} [nm/RIU]	*f*	*Q*	λ_0 [nm]	S_{SMM} [nm/RIU]	S_{Meep} [nm/RIU]	*f*	*Q*
100	1588	170	149	0.158	3712	1506	238	291	0.287	123484
200	1552	211	212	0.221	347	1498	238	222	0.224	8762
300	1516	248	310	0.315	111	1478	223	205	0.207	2798
350	1498	260	354	0.355	83	1466	166	163	0.164	2941
300 (t=180nm)	1487	213	268	0.272	186	1460	38	74	0.074	14343

The effects of the substrate are further pronounced when considering asymmetric designs with a thin PCS, as shown in the bottom row in Table 2. Figure 6 shows electric field energy density profiles for a thin PCS with a thickness of 0.18*a* and radius of 0.3*a* for the asymmetric [(a), (c)] and the symmetric designs [(b), (d)]. The ability of the PCS to support *bona fide* guided resonance modes degrades as the slab is made thinner. The result is less electric field energy being constrained to the slab and significantly more energy present in the substrate. In both the TE- and TM-like cases, the substrate contains a large portion of the electric field energy, as the *f* values of the last row of Table 2 confirm.

The perceived sensitivity enhancement due to the reduction of n_{eff} by thinning the PCS (as predicted by Eq. (2)) is offset by the substantial reduction of *f* that is observed. As the PCS is made thinner, modes will be more poorly confined to the dielectric. A cutoff condition is reached when the PCS is too thin to support a guided resonance mode. In this situation, the electric field radiates through the slab.

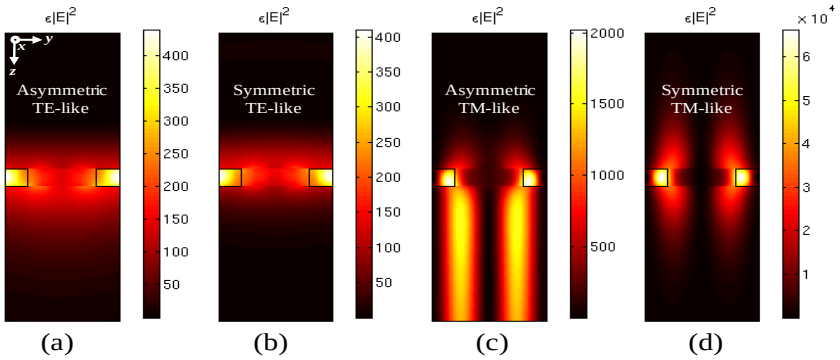

Fig. 6. Guided resonance mode profile for a thin slab (t = 180 nm) PCS. The electric field energy density, $\varepsilon|E|^2$, is shown for the cases: (a) TE-like resonance in an asymmetric PCS, (b) TE-like resonance in a symmetric PCS, (c) TM-like resonance in an asymmetric PCS and (d) TM-like resonance in a symmetric PCS. The electric field energy density profiles were calculated using the SMM method for hole radius to period ratio (r/a) = 0.3.

An additional practical consideration is the linearity of the relationship between changes in guided resonance spectral location and surrounding RI. This proportionality is valid only as a first-order approximation. As the surrounding RI value exits the range in which the approximation is valid, non-linear behavior is observed as shown in Fig. 7. Capitalizing on this non-linearity may be difficult in practice as we are primarily concerned with interrogating fluids with RI values close to that of water. The significance of the data presented in Fig. 7,

#131867 - $15.00 USD Received 19 Jul 2010; revised 7 Sep 2010; accepted 20 Sep 2010; published 12 Oct 2010

however, is the observed trend that longer wavelength guided resonances will have a higher sensitivity.

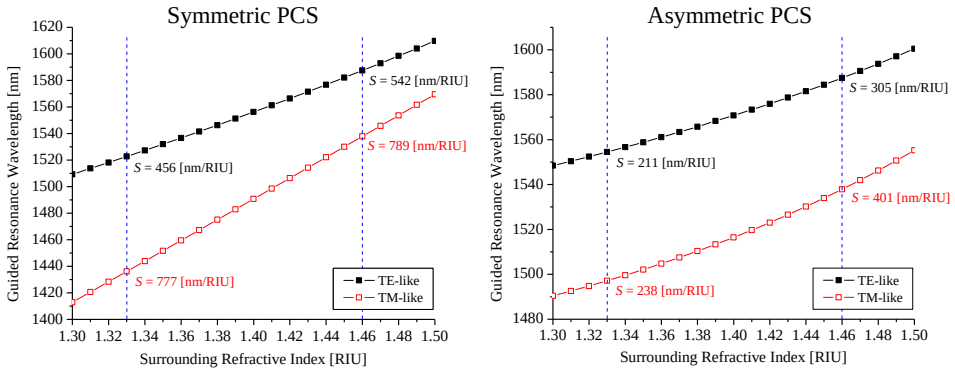

Fig. 7. Guided resonance wavelength versus surrounding RI for a (a) symmetric PCS sensor design and an (b) asymmetric PCS sensor design (r = 300 nm, t = 250 nm). Bulk spectral sensitivity values are indicated for surrounding RI values of 1.33 and 1.46.

6. Biosensing

At a system level, the PCS biosensors which we analyze provide significant advantages. Our analysis demonstrates that a high Q is not a requisite for high spectral sensitivity. As indicated by Eq. (3) and in previous studies evaluating other types of photonic biosensors [44,45], a much better figure of merit is a high value for the product of Q and S. This trait is especially evident for symmetric designs and may greatly reduce fabrication constraints. CMOS compatibility and the availability of integrated laser/detector readout modules make miniaturized PCS biosensing solutions viable. Additionally, a large photonic crystal hole array may be patterned to provide both simple light coupling from free space and a rich functionalized area for biosensing.

Table 3 compares the sensing attributes of the analyzed 200 nm hole radius symmetric and asymmetric PCS designs to simulations of currently existing large-area photonic biosensing platforms. These include the SPR sensors described by Homola *et al.* [46] and the one-dimensional grating sensors described by Block *et al.* [30]. A PCS-based biosensor can offer a similar (or potentially smaller, for TM-like guided resonances) *DL* as compared to these large area biosensors. Furthermore, they offer reduced polarization sensitivity, narrower lineshapes [36] and guided mode selection as an optimization parameter depending on the analyte type.

Table 3. Comparison of symmetric and asymmetric PCS biosensors to SPR sensor [46] and one-dimensional grating sensor [30] simulations.

Sensing Metric	SPR	1DG	Asymmetric PCS (r = 200 nm)		Symmetric PCS (r = 200 nm)	
			TE-like	TM-like	TE-like	TM-like
Q	50	741.3	347	8762	313	16240
***S* [nm/RIU]**	3000	394	211	238	456	777
***DL* [RIU]**	$\sim 10^{-6}$	$\sim 10^{-6}$	$\sim 5 \cdot 10^{-6}$	$\sim 10^{-7}$	$\sim 10^{-6}$	$\sim 10^{-7}$-10^{-8}

Measured Q values may be lower than those predicted from simulations partly due to hole roughness and shape irregularities. Additionally, PCS structures resting on or above a substrate will have superimposed Fabry-Pérot interference which can be numerically filtered out from experimental transmission data, but only at the expense of reducing the otherwise inherently high Q values. Hence, this introduced measurement uncertainty is expected to be reduced in suspended, substrateless PCS structures. Measured Q values may be further improved with crossed-polarization transmission measurements, which distinguish guided

#131867 - $15.00 USD Received 19 Jul 2010; revised 7 Sep 2010; accepted 20 Sep 2010; published 12 Oct 2010

resonances clearly in the form of pure Lorentzians, facilitating the measurement of high *Q* values and greatly attenuating substrate-imposed Fabry-Pérot interference [20,42]. Our initial experimental studies have indicated *Q* values greater than 10^3 on TM-like modes for asymmetric PCS structures with ± 2 nm deviations in hole diameters and slight non-uniformities in etch profile. Based on our analysis, we expect the *DL* to improve to ~10^{-8} [RIU] with symmetric designs.

The fragility of suspended PCS membranes in symmetric PCS designs can be curtailed with circular PCS patterns to evenly distribute embedded stress. Our analysis concerns 250 nm-thick SiN_x films which are sufficient for maintaining low stress levels for robust PCS fabrication. Previous works have reported 50 nm-thick SiN_x PCS membranes suspended in water-based solutions [33].

The analysis presented in this paper concerns bulk sensitivity, i.e., monitoring changes in resonance spectral location when the entire RI of the surrounding fluid is changed. This complements analysis of mode profiles and field overlaps, and is a meaningful figure of merit when considering the sensing of large analytes, such as cells and bacteria, which may be represented by a bulk RI [47]. Another important metric is the sensitivity of resonances with respect to RI changes in a layer in close proximity to the surface of the PCS, otherwise known as the detection zone [30]. In an ideal scenario, the resonant mode will overlap the active binding region for analytes within the detection zone. This metric, referred to as the surface spectral sensitivity, represents the change of RI that occurs due to analytes binding to a functionalized PCS biosensor. The depth of the detection zone from the RI sensor surface depends on the detected analyte and can be ~25 nm for detecting large proteins [30], ~100 nm when using a textured surface (for example, by nano-rods or permeable organic or inorganic nano-cavities), and on the order of few microns when detecting changes inside cells [13,48].

Another important consideration is the size of the detection area. Increased sensor surface area can reduce the duration of biodetection, improve the fidelity of statistics when evaluating binding kinetics and improve sensitivity. We have shown PCS sensor areas as large as 15 x 15 mm [31] while others have demonstrated even larger one-dimensional PC structures with areas of 75 x 125 mm [49].

Equation (2) represents a linear relationship between the *S* and the resonance wavelength. A design tailored to NIR wavelengths (~750 nm) is expected to have roughly half the sensitivity of a corresponding design centered in the communication band (~1550 nm). The mode profiles and PCS dimensions scale accordingly, and allow flexibility in determining an appropriate mode volume. A PCS optimized for NIR wavelengths enjoys the benefit of spectral matching to NIR fluorescent molecules or quantum dot markers, and can also be used to enhance the excitation or fluorescence of these markers [50]. Furthermore, NIR-tailored designs offer compatibility with previously proposed laser/detector modules, for direct integration into microfluidic platforms [51].

As explained above, optimization of a PCS biodetection assay requires proper mode selection to ensure a good match between the detection zone and the electric field energy profile. This implies that sensors with a poor electric field energy overlap with the detection zone will result in reduced sensitivity, similar to reducing *f* in our analysis. On the other hand, if the electric field energy profile extends beyond the detection zone for a particular analyte of interest, the sensitivity will not be enhanced, to the contrary it may degrade by added external noise due to fluctuations of the bulk RI [30]. While TM-like resonances exhibit a large *S*, the large vertical field penetration they exhibit should match the sensing target of interest. It is well suited for detection of bacteria and cells (to minimize the out-of-detection-zone electric field mode volume), and can also be used for detection of proteins and enzymes with the addition of hydrogel matrices above the PCS, a common practice for SPR sensors [52]. The mode profile of TE-like resonances, however, extends less to external regions, and may be better optimized for protein and enzyme detection assays. The ability to optimizing the energy profile for a wide range of analytes is yet another unique property of PCS biosensors.

#131867 - $15.00 USD Received 19 Jul 2010; revised 7 Sep 2010; accepted 20 Sep 2010; published 12 Oct 2010

7. Conclusion

We have presented a theoretical analysis of guided resonances in PCS structures for biosensing. We discuss the differences between TE-like and TM-like modes, and their implications in bulk spectral sensitivity and resonance quality factors. We have reviewed the underlying physics and the engineering aspects in selecting a symmetric or asymmetric PCS topology. It is demonstrated that PCS biosensors suspended over a substrate (symmetric designs) can display roughly a three-fold increase in bulk sensitivity over slab-on substrate architectures (asymmetric designs) for TM-like guided resonances. Furthermore, we report that TM-like guided resonances have a stronger vertical field penetration than TE-like guided resonances, which contributes to their significantly higher bulk index sensitivity and to their potential to overcome major fabrication-related challenges in realizing high quality factors in large area PCS sensors. PCS sensors can have similar (TE-like) or smaller (TM-like) detection limits compared to existing optical biosensing techniques, with the added advantages of sensitivity optimization based on mode selection, and straight-forward sensor integration with microfluidics and optical readout by free space beams. Finally, analysis of modal field distributions suggest that TE-like resonance sensors may be suited for protein and biomolecule detection while TM-like resonance sensors are more meaningful for use to sense cells and large analytes.

Acknowledgements

The authors are grateful for the helpful discussions with O. Kilic and W. Suh during the early parts of this project. This work was supported in part through the University of Toronto departmental start-up funds to O. Levi, the Natural Sciences and Engineering Research Council of Canada (NSERC) Discovery Grant RGPIN-355623-08 and by the Networks of Centres of Excellence of Canada, Canadian Institute for Photonic Innovations (CIPI). V. Liu acknowledges partial graduate fellowship support by a Stanford Graduate Fellowship. Funding for M. El Beheiry was provided in part by the Ontario Graduate Scholarship Program and the Edward S. Rogers Sr. Graduate Scholarship.

#131867 - $15.00 USD Received 19 Jul 2010; revised 7 Sep 2010; accepted 20 Sep 2010; published 12 Oct 2010